DEVELOPMENT OF A LIFE-CYCLE ASSESSMENT TOOL FOR PAVEMENT PRESERVATION AND MAINTENANCE

FINAL PROJECT REPORT VOLUME II

by

Egemen Okte
Qingwen Zhou
Sushobhan Sen
Shabnam Rajaei

Hasan Ozer
Imad L. Al-Qadi
Jeffery R. Roesler
Karim Chatti

The Illinois Center for Transportation (ICT) of the University of Illinois at Urbana-Champaign
Michigan State University

for

Center for Highway Pavement Preservation
(CHPP)

Disclaimer

The contents of this report reflect the authors' views — all of whom are responsible for the facts and accuracy of the data presented herein. The contents do not necessarily reflect the official views or policies of the Illinois Center for Transportation (ICT). This report does not constitute a standard, specification, or regulation. Trademark or manufacturers' names appear in this report as they are essential to the document's objective and do not constitute an endorsement of product by ICT.

Technical Report Documentation Page			
1. Report No. CHPP Report-UIUC#7-2019	2. Government Accession No.	3. Recipient's Catalog No.	
4. Title and Subtitle Development of a Life-Cycle Assessment Tool for Pavement Preservation and Maintenance on Flexible and Rigid Pavement		5. Report Date	
		6. Performing Organization Code	
7. Author(s)		8. Performing Organization Report No.	
9. Performing Organization Name and Address Center for Highway Pavement Preservation, Tier 1 University Transportation Center Michigan State University, 2857 Jolly Road, Okemos, MI 48864		10. Work Unit No. (TRAIS)	
		11. Contract or Grant No.	
12. Sponsoring Organization Name and Address		13. Type of Report and Period Covered	
		14. Sponsoring Agency Code	
15. Supplementary Notes			

16. Abstract

Volume II details the background and explanation of models applied in the use stage and work zone of life cycle assessment (LCA) on pavement preservation and maintenance schedules. A pavement's LCA use stage generally includes roadway lighting, carbonation, heat island effect and rolling resistance. Roadway lighting and carbonation are not included in calculations because of the high variability of parameters used to calculate these impacts and their relatively low effect.

In this study, only heat island impacts and rolling resistance are considered in use stage. This study introduces methods to calculate extra energy consumption and environmental impacts due to work zone traffic delay. For heat island impact, different albedo values are assigned to different surface treatments. Global warming potential (GWP) can be calculated, in tons of CO_2, using the radioactive forcing of the corresponding state of the project.

Impacts due to roughness include energy consumption, GWP, smog, and other environmental impacts can be captured by a roughness speed impact (RSI) model. Three different models capture roughness progression, and they include: (1) the default model in which the user is required to input the initial and threshold International Roughness Index (IRI) values for the surface treatments, (2) basic linear model in which the user is required to input the IRI progression rate for the project, and (3) an advanced model in which the user is required to input the progression model parameters that depend on traffic levels and surface thickness.

An extensive literature survey captures texture progression, and it is assumed that the texture measured in mean profile depth (MPD), stays constant for the life of the treatment. The regression model captures impacts due to texture and is based on the calibrated Highway Development and Management Model (HDM-4). Energy consumption is calculated and used to determine GWP and other impacts.

Impacts due to work zone traffic delay follow the same models as roughness impact calculation. The user is required to input traffic information (i.e. work zone speed and length and normal traffic speed) to capture the difference of impacts under work zone and normal traffic flows.

17. Key Words		18. Distribution Statement No restrictions.	
19. Security Classification (of this report) Unclassified.	20. Security Classification (of this page) Unclassified.	21. No. of Pages	22. Price N/A

Form DOT F 1700.7 (8-72) Reproduction of completed page authorized

Table of Contents

List of Figures

List of Tables

List of Abbreviations

AC	Asphalt concrete
ASTM	American Society for Testing and Materials
EPA	Environmental Protection Agency
GWP	Global warming potential
HDM-4	Highway Development Management Model
HMA	Hot mix asphalt
IRI	International Roughness Index
ISO	International Organization for Standardization
LCA	Life-cycle assessment
LTPP	Long-Term Pavement Performance
MIRIAM	Models for rolling resistance In Road Infrastructure Asset Management Systems
MOVES	Motor vehicle emission simulator
MPD	Mean profile depth
NCHRP	National Cooperative Highway Research Program
PCC	Portland cement concrete
PSAT	Preservation sustainability assessment tool
RF_p	Radiative forcing
RR	Rolling resistance
RSI	Roughness speed impact
TRACI	Tool for the Reduction and Assessment of Chemical and other environmental Impacts
VSP	Vehicle specific power

Acknowledgments

The authors would like to acknowledge the financial support of the Center for Highway Pavement Preservation.

Executive Summary

Volume II details the background and explanation of models applied in the use stage and work zone of life cycle assessment (LCA) on pavement preservation and maintenance schedules. A pavement's LCA use stage generally includes roadway lighting, carbonation, heat island effect and rolling resistance. Roadway lighting and carbonation are not included in calculations because of the high variability of parameters used to calculate these impacts and their relatively low effect.

In this study, only heat island impacts and rolling resistance are considered in use stage. This study introduces methods to calculate extra energy consumption and environmental impacts due to work zone traffic delay. For heat island impact, different albedo values are assigned to different surface treatments. Global warming potential (GWP) can be calculated, in tons of CO_2, using the radioactive forcing of the corresponding state of the project.

Impacts due to roughness include energy consumption, GWP, smog, and other environmental impacts can be captured by a roughness speed impact (RSI) model. Three different models capture roughness progression, and they include: (1) the default model in which the user is required to input the initial and threshold International Roughness Index (IRI) values for the surface treatments, (2) basic linear model in which the user is required to input the IRI progression rate for the project, and (3) an advanced model in which the user is required to input the progression model parameters that depend on traffic levels and surface thickness.

An extensive literature survey captures texture progression, and it is assumed that the texture measured in mean profile depth (MPD), stays constant for the life of the treatment. The regression model captures impacts due to texture and is based on the calibrated Highway Development and Management Model (HDM-4). Energy consumption is calculated and used to determine GWP and other impacts.

Impacts due to work zone traffic delay follow the same models as roughness impact calculation. The user is required to input traffic information (i.e. work zone speed and length and normal traffic speed) to capture the difference of impacts under work zone and normal traffic flows.

CHAPTER 1 - INTRODUCTION

Estimated energy consumption of traffic throughout a roadway's lifetime is around 95 to 98 percent; if the analysis period exceeds 20 years (Araújo et al, 2014). It is also estimated that road transport is one of the largest contributors of CO_2 emissions, accounting up to 30 percent of transportation-related emissions (Pérez-Martínez, 2012).

To assess the sustainability of a road surface, all stages of a pavement project should be incorporated in the life cycle assessment (LCA). These stages are materials, construction, maintenance and rehabilitation, use, and end of life. All stages, with the exception of the use stage, are direct results of agency decisions on the materials used, road geometry, and construction schedule. Use stage on the other hand directly incorporates the impact of the users driving on the roadway. The majority of traditional LCA methodologies exclude the use stage, which neglects a large portion of emissions. The most significant factors that contribute to energy consumption during the use stage are: carbonation of concrete rigid pavements, lighting of the pavement surface (if any), heat islands, and rolling resistance.

Carbonation is the process of CO_2 absorption of concrete pavements over time. Water to cement ratio, temperature, and relative humidity might affect the carbonation process. Carbonation is not included in this study. Heat islands involve a roadway surface's ability to reflect solar radiation, which varies from zero, for total absorption, to one, for reflectance. Depending on the reflectivity, each surface has a corresponding global warming potential (GWP). Heat island impacts for different states around the U.S. are considered in the study.

Rolling resistance is the energy loss due to interaction between pavement and the vehicle, which is related to vehicle parts and pavement conditions. Rolling resistance may occur due to pavement roughness and macro-texture (refers to herein as texture). Additionally, rolling resistance impact require progression models. This study considers progression and impact models for both roughness and texture.

In addition, whenever a traffic disturbance, such as a work zone, occurs, energy consumption increases. This increase is due to vehicles slowing down before, queueing during, and speeding up after work zones. Additional impact is related to vehicle operation; vehicle idling consumption, depending on the duration, could be quite significant.

Volume II of the report explains heat islands, rolling resistance, and work-zone-related impacts and their calculations.

CHAPTER 2 - USE STAGE IMPACT MODELS

2.1 HEAT ISLAND IMPACT

2.1.1 Background

Pavement heat island impacts are controlled by thermal and optical properties. The optical properties and their impacts are the following:

1. Albedo or average solar reflectance: determines the fraction of incoming short-wave solar radiation reflected by the pavement. The rest is absorbed and thermalized, which increases pavement surface temperature. This is a surface property.
2. Emissivity: determines the amount of long-wave energy emitted out of the pavement surface to the atmosphere or surroundings. This is also a surface property.

On the other hand, the thermal properties and their impacts are the following:

1. Thermal conductivity (W/mK): the amount of heat transmitted by each pavement layer per unit time, temperature, and thickness. This is a volumetric property.
2. Heat capacity (J/m^3K): the amount of heat a unit volume of pavement material must absorb for a unit increase in temperature. It is also a volumetric property.
3. Thermal diffusivity (m^2/s): the thermal conductivity divided by the heat capacity. This is a fundamental parameter in heat transfer. It controls how quickly heat energy diffuses through the different pavement layers, and it influences the temperature profile. It is also a volumetric property.

The project goal was to measure the thermal and optical properties of typical pavement materials — specifically, the following materials:

1. Asphalt concrete (AC) obtained from field cores,
2. Chip seals obtained from field cores, and
3. Portland cement concrete (PCC) samples prepared in the lab with various mix designs.

Optical properties were determined using a spectrophotometer. The albedo was calculated as per ASTM E1918 in conjunction with ASTM G173, while the emissivity was determined as per Method C specified in ASTM E408. The thermal properties were evaluated using a rapid Transient Plane Source technique based on the work of Gustafsson (1991).

In a previous study (Sen and Roesler, 2017), microscale heat island metric pavement Radiative Forcing (RF_p) and a corresponding Global Warming Potential (GWP) were introduced. Another study (Sen and Roesler, 2016) showed how the heat island impact of pavement preservation techniques varied by service life and geographic location. Based on these two methods, the GWP of various pavement preservation options available to users was evaluated in terms of equivalent kg CO_2/m^2 of pavement. Evaluation of pavements occurred in each state, using representative weather data from cities approximately along the latitude that bisects the state into two. In the case of two "long" states, including California and Texas, three separate cities — North, Central, and South — were chosen for analysis. Thus, the heat island impact of 54 total cases (48 states + three

Texas cities + three California cities) were evaluated for each pavement preservation treatment available to the user.

2.1.2 Model Development

The most important factor in determining the GWP — a long-term heat island metric — is albedo. Pavement preservation treatments were classified into three groups (as shown in Table 2-1). AC-based surface treatments had a low albedo of 0.05, while treatments involving AC-based overlays or modifications to AC surfaces that covered only a small area, such as crack sealing, had an albedo of 0.20. This corresponds to AC that is at least one year old, which is typical for pavement preservation (Sen and Roesler 2016). Finally, concrete treatments were assigned an albedo of 0.30, corresponding to typical PCC albedo.

Table 2-1 Assigned Albedo Values for Different Treatment Types

Group No.	Treatment	Assigned albedo
1	Slurry seal	0.05
	Chip seal	
	Microsurfacing	
2	Crack filling	0.20
	Crack sealing	
	Thin HMA overlay	
	Ultra-thin HMA overlay	
	Hot-in-place recycling	
	Cold-in-place recycling	
	Ultra-thin bonded wearing course	
3	Slab stabilization	0.30
	Slab jacking	
	Partial-depth repair	
	Dowel-bar retrofitting	
	Diamond grinding	
	Joint and crack resealing	
	BCOA and FFC inlays	

The RF_p of each group of treatments was determined assuming the following pavement geometry:

Groups 1 and 2: 8 in AC, 10 in A-3 base A-6 subgrade.

Group 3: 8 in the PCC, 10 in A-3 base, and A-6 subgrade.

Given that the RF_p, a long-term metric, only depends on albedo and not the thermal properties or geometry of the pavement layers, the result depends only on albedo. The RF_p was calculated using the ILLI-THERM program (Sen and Roesler, 2017). Using the RF_p, the GWP was calculated using the following equation:

$$GWP(t) = \frac{A \times RF_p \times \ln 2 \times P_{CO_2} \times M_{CO_2} \times m_{air}}{A_{earth} \times \Delta F_{2x} \times M_{air} \times AF(t)} \quad (2.1)$$

where,

A is area of the road (use 1 m^2);
RF_p is pavement forcing from the database;
P_{CO_2} is reference CO_2 partial pressure (383 ppmv = 383 x 10^{-6});
M_{CO_2} is molecular weight of CO_2 (44 g/mol);
m_{air} is total mass of atmosphere (5.148 × 10^{21} g);
A_{earth} is surface area of earth (5.1 × 1014 m^2);
ΔF_{2x} is increase in RF_p due to doubling ambient concentration of CO_2 (use 3.7 W/m^2);
M_{air} is molecular weight of dry air (28.95 g/mol); and
$AF(t)$ is average CO_2 airborne fraction after t years.

$AF(t)$ can be expressed as follows:

$$AF(t) = \frac{1}{t}\int_0^{\tau} f(\tau)d\tau \quad (2.2)$$

$$= \frac{51.3834 - 0.34596e^{-0.537634t} - 6.25638e^{-0.0540249t} - 44.7811e^{-0.00578369t} + 0.217t}{t}$$

$$f(t) = 0.217 + 0.259e^{-\frac{t}{172.9}} + 0.338e^{-\frac{t}{18.51}} + 0.186e^{-\frac{t}{1.86}} \quad (2.3)$$

Here, *t* corresponds to the treatment's years of service life.

The RF_p for each state, corresponding city, and airport used to obtain weather data for its calculation is shown in the table below. The PSAT tool uses this value for each treatment option and calculates the GWP based on the service life.

Table 2-2 RF_p Factors for Each State

No.	State	Code	City	Airport	RF_p (W/m^2)		
					Group 1	Group 2	Group 3
1	Alabama	AL	Alabaster	Shelby County Airport	80.81	58.45	42.65
2	Alaska	AK	Anchorage	Ted Stevens Anchorage International Airport	32.74	21.24	9.76
3	Arizona	AZ	Prescott	Prescott Regional Airport	93.84	68.02	50.66
4	Arkansas	AR	Little Rock	Bill and Hillary Clinton National Airport	66.32	47.62	34.88

No.	State	Code	City	Airport	RF_p (W/m^2)		
					Group 1	Group 2	Group 3
5	California N	CAN	Redding	Redding Municipal Airport	81.81	58.94	43.73
6	California C	CAC	Hanford	Hanford Municipal Airport	88.48	63.24	46.61
7	California S	CAS	Los Angeles	Los Angeles International Airport	82.80	60.90	46.95
8	Colorado	CO	Colorado Springs	City of Colorado Springs Municipal Airport	81.79	59.23	44.34
9	Connecticut	CT	Hartford	Hartford-Brainard Airport	73.70	53.41	39.96
10	Delaware	DE	Georgetown	Delaware Costal Airport	86.76	62.66	46.71
11	Florida	FL	Orlando	Orlando Sanford International Airport	84.05	58.91	42.80
12	Georgia	GA	Macon	Middle Georgia Regional Airport	81.15	58.18	42.62
13	Hawaii	HI	Kailua Kona	Kona International Airport	105.92	76.86	59.07
14	Idaho	ID	Boise	Boise Airport	84.96	61.28	45.94
15	Illinois	IL	Champaign	Willard Airport	74.19	53.31	39.64
16	Indiana	IN	Indianapolis	Indianapolis International Airport	59.29	43.19	32.42
17	Iowa	IA	Ames	Ames Municipal Airport	79.05	58.16	44.00
18	Kansas	KS	Salina	Salina Regional Airport	85.34	61.53	46.16
19	Kentucky	KY	Jackson	Julian Carroll Airport	76.84	55.78	42.55
20	Louisiana	LA	Alexandria	Alexandria Esler Regional Airport	80.64	58.05	41.89
21	Maine	ME	Millinocket	Millinocket Municipal Airport	69.20	50.94	37.29
22	Maryland	MD	Baltimore	Baltimore-Washington International Thurgood Marshall Airport	61.98	45.20	33.60

No.	State	Code	City	Airport	RF_p (W/m^2)		
					Group 1	Group 2	Group 3
23	Massachusetts	MA	Worcester	Worcester Regional Airport	76.77	55.74	41.85
24	Michigan	MI	Grand Rapids	Gerald R. Ford International Airport	67.27	49.62	38.07
25	Minnesota	MN	St. Cloud	St. Cloud Regional Airport	73.65	52.99	40.18
26	Mississippi	MS	Meridian	Meridian Regional Airport	83.90	60.69	44.60
27	Missouri	MO	Jefferson City	Jefferson City Memorial Airport	83.64	60.56	45.45
28	Montana	MT	Lewistown	Lewistown Municipal Airport	75.62	54.90	41.10
29	Nebraska	NE	Cheyenne, WY	Cheyenne Regional Airport	85.76	62.33	46.89
30	Nevada	NV	Winnemucca	Winnemucca Municipal Airport	86.94	63.21	47.39
31	New Hampshire	NH	Concord	Concord Municipal Airport	72.07	52.60	39.21
32	New Jersey	NJ	Atlantic City	Atlantic City International Airport	84.88	61.53	46.16
33	New Mexico	NM	Albuquerque	Albuquerque International Sunport	81.40	58.94	44.93
34	New York	NY	Utica	Oneida County Airport (closed)	77.89	58.36	45.80
35	North Carolina	NC	Raleigh	Raleigh-Durham International Airport	64.36	46.69	34.30
36	North Dakota	ND	Bismarck	Bismarck Airport	71.69	51.44	36.57
37	Ohio	OH	Newark	Newark-Heath Airport	77.16	56.83	42.81
38	Oklahoma	OK	Guthrie	Guthrie-Edmond Regional Airport	89.09	63.86	47.73
39	Oregon	OR	Redmond	Redmond Municipal Airport	81.16	58.95	44.07
40	Pennsylvania	PA	Clearfield	Clearfield-Lawrence Township Airport	86.24	65.04	51.44
41	Rhode Island	RI	Providence	T.F. Green Airport	68.72	50.18	38.02

No.	State	Code	City	Airport	RF_p (W/m^2)		
					Group 1	Group 2	Group 3
42	South Carolina	SC	Columbia	Columbia Metropolitan Airport	84.90	61.13	45.23
43	South Dakota	SD	Pierre	Pierre Regional Airport	79.94	57.59	42.64
44	Tennessee	TN	Nashville	Nashville International Airport	63.52	46.45	34.63
45	Texas N	TXN	Amarillo	Rick Husband Amarillo International Airport	93.56	67.82	51.28
46	Texas C	TXC	Dallas	Dallas/Fort Worth International Airport	71.85	51.03	37.64
47	Texas S	TXS	Corpus Christi	Corpus Christi International Airport	85.93	61.30	45.67
48	Utah	UT	Price	Carbon County Regional Airport	93.77	68.54	52.21
49	Vermont	VT	Montpelier	Edward F. Knapp State Airport	70.53	52.37	38.34
50	Virginia	VA	Lynchburg	Lynchburg Regional Airport	81.31	59.11	43.79
51	Washington	WA	Yakima	Yakima Air Terminal	74.83	53.10	38.99
52	West Virginia	WV	Elkins	Elkins-Randolph Co. Regional Airport	74.60	56.45	43.02
53	Wisconsin	WI	Marshfield	Marshfield Municipal Airport	74.63	54.59	40.90
54	Wyoming	WY	Riverton	Riverton Regional Airport	88.87	64.73	49.39

2.2 ROLLING RESISTANCE IMPACT

2.2.1 Background

Rolling Resistance (RR) is the loss of energy per unit distance travelled as defined by ISO 28580 (ISO, 2009). Air resistance, vehicle inertial resistance, road-gradient resistance, side-force resistance, transmission losses, and engine friction are known to affect the RR. Tire properties, pavement structure, and surface geometry, coupled with vehicle dynamics, also affect RR (Lepert and Brillet, 2009).

Because RR contributes almost 20 percent of transportation-related consumption, according to International Energy Agency's 2005 report, it is crucial to quantify the impact of RR. Pavement roughness and texture are the two main components of RR related consumption (Jackson et al, 2011), and they should be considered separately.

Pavement roughness is the lack of smoothness, or unevenness of the pavement surface. It is generally a function of construction quality and traffic. The IRI is commonly used to measure roughness. IRI is calculated by running a quarter car simulation on the road surface profile and recording the vertical displacement of a vehicle each mile, and therefore its unit is in/mi. IRI strongly correlates with RR. High roughness increases fuel consumption of any type of vehicle, as much as 20 percent (Chatti and Zaabar, 2012).

Texture, on the other hand, corresponds to smaller wavelengths than pavement roughness, and it is a primary characteristic of the pavement surface that controls friction and sound. Texture is usually provided by the characteristics of the surfacing materials, such as aggregates for AC pavements. Texture affects RR resistance of vehicles. Its effect increases with heavier vehicles, such as articulated trucks; whereas for light vehicles, such as passenger vehicles, its effect may be negligible (Chatti and Zaaba, 2012).

This study utilized the roughness speed impact (RSI) model for quantifying roughness-related RR resistance (Ziyadi et al, 2018). The RSI model estimates additional energy consumption due to pavement roughness. Experiment-based results from the National Cooperative Highway Research Program (NCHRP) were used to quantify texture related RR (Zaabar and Chatti, 2012).

2.2.2 Roughness-Related Rolling Resistance

To quantify fuel consumption due to roughness, the World Bank developed the HDM-4, which is based on mechanistic principles of vehicle specific power (VSP). However, the model used in HDM-4 needed calibration for various speeds and vehicle types. Even though many researchers conducted calibrations — given that these calibrations require experimental data — the model could only be calibrated for certain speeds and vehicle types.

Alternatively, the U.S. Environmental Protection Agency (EPA) developed the motor vehicle emission simulator (MOVES), which quantifies the energy consumption of various types of vehicles with a wide range of factors; such as age, technology, fuel type, and road grade. Unfortunately, MOVES does not account for pavement surface conditions. Ghosh et al. (2015) incorporated the effects of pavement roughness into MOVES simulations by running different cases under various conditions. However, the study failed to develop a generalized formulation based on the MOVES simulations, and thus its results were only case specific.

In an attempt to create a generalized model that accounts for pavement roughness, this study created a roughness speed impact model (RSI), proposed by Ziyadi et al. (2018), using previously developed MOVES simulations corresponding to HDM-4 models. The first step fitted vehicle-specific power and energy per distance traveled to develop energy consumption model as presented in equation (2.3).

$$RSI_{t=0}^{Energy}: \hat{E}(v, IRI) = \frac{p}{v} + (k_a.IRI + d_a) + b \times v + (k_c.IRI + d_c) \times v^2 \qquad (2.4)$$

where,

$\widehat{E}(v, IRI)$: Estimated energy consumption per vehicle distance (kJ/mi)
v: Speed of the vehicle in mph
IRI: International Roughness Index in in/mi.
$k_a, d_a, k_c, d_c, p \text{ and } b$: Regression coefficients which are presented in Table 2-3.

The next step was to formulate the relationship covering a full list of environmental impacts at various vehicle speeds and IRIs. A model was developed to calculate the reduction, assessment of chemicals and other environmental impacts (TRACI). Instead of computing the absolute value of emissions and impacts, an alternative method that focuses on the increment rate of pollutants changing with vehicle speed and IRI was adopted. The model formulated the increment value due to pavement roughness change as the percent increment (q_{vi}) of environmental impact over the baseline TRACI impact at IRI=0 and given speed (v), as presented in equation (2.4). The total TRACI impact i at given speed v and pavement roughness IRI can be computed by summing the baseline impact i and the increment value, shown in equation (2.5).

$$\Delta RSI_{t=0}^{Env}: \Delta\hat{I}(v, \Delta IRI) = \left[q_{v_i}.\frac{\Delta IRI}{63.36}\right] * I_i(v) \quad (2.5)$$

$$RSI_{t=0}^{Env}: \hat{I}(v, IRI) = I_i(v) + \Delta\hat{I}(v, \Delta IRI) \quad (2.6)$$

where,

$\hat{I}(v, IRI)$: Estimated total TRACI impact i per vehicle distance (mi) at given speed v (mph) and pavement roughness IRI (in/mi)
$\Delta\hat{I}(v, \Delta IRI)$: Estimated additional TRACI impact i per vehicle distance (mi) at given speed v (mph) due to change in pavement roughness ΔIRI (in/mi)
$I_i(v)$: Baseline TRACI impact i at given speed v (mph) and IRI = 0
ΔIRI : Change in IRI (in/mi)
q_{vi}: Percent increment of the environmental impact i at speed v (mph), which can be computed by equation (2.6)

$$q_{v_i} = k_{v_i} \times v + d_{v_i} \quad (2.7)$$

k_{v_i}, d_{v_i} are increment rate coefficients. Table 2-4 presents the model coefficients for passenger cars per the TRACI impact category. Ozone and fossil fuel depletions are not included because MOVES simulations showed those two impacts are not affected by pollutants used in the developed RSI model.

To validate the model, it was compared to mainly the calibrated HDM-4 and MOVES models. Figure 2-1 illustrates the comparison between the developed model and the HDM-4 and MOVES models. The results indicate a strong correlation between the IRI and higher speed energy consumptions.

Table 2-3 RSI Energy Model Coefficients

Coefficients	Passenger car	Small truck	Medium truck	Large truck
ka	6.70E-01	7.68E-01	9.18E-01	1.40E+00
kc	2.81E-04	1.25E-04	1.33E-04	1.36E-04
dc	2.1860E-01	3.0769E-01	9.7418E-01	2.3900E+00
da	2.1757E+03	7.0108E+03	9.2993E+03	1.9225E+04
b	-1.6931E+01	-7.3026E+01	-1.3959E+02	-2.6432E+02
p	3.3753E+04	1.1788E+05	1.0938E+05	8.2782E+04

Table 2-4 Increment Rate Coefficients for Passenger Vehicles

Impact Category i	k_{v_i}	d_{v_i}
Global warming	5.88E-4	3.51E-3
Smog	8.06E-4	1.42E-2
Acidification	7.83E-4	1.25E-2
Eutrophication	7.83E-4	1.27E-2
Carcinogenics	7.24E-4	-7.24E-3
Noncarcinogenics	7.59E-5	-9.25E-4
Respiratory effects	1.01E-3	2.8E-3
Ecotoxicity	1.8E-4	-2.05E-3

2.2.3 Texture Effect on Rolling Resistance

The macro-texture related energy model, developed by Zaabar and Chatti (2012), used in this study, utilizes a regression model and calibrates the original HDM-4 models with field tests. It accounts for texture effect on heavy vehicles. The equation for this model requires only one input, the vehicle's speed (v) in mph (Zaabar and Chatti, 2012).

$$\delta Etexture\ (\%) = 0.02 - 2.5 \times 10{-}4 \times (v{-}35) \tag{2.8}$$

To verify the developed model, it was compared to In Road Infrastructure Asset Management Systems (MIRIAM) and Boere models. The MIRIAM model was proposed based on a previously modified model using coast down measurements in Sweden (Karlsson et al. 2011). The RR model was established considering variation of the MPD, IRI, temperature, and speed for a car, heavy truck, and a heavy truck with trailer. Mean profile depth (MPD) values ranged from 0.25 to 2.7 mm (0.01 to 0.1in). On the other hand, the Boere model is a mechanistic model and accounts for the tire-pavement surface interaction by applying a nonlinear contact stiffness to the roadway (Boere, 2009).

Figure 2-2 shows the comparison of the adjustment factors for RR resistance between the NCHRP 720 and Boere models for a light truck (4.1t). The NCHRP 720 and the experimental results reported by Boere are similar. Boere's numerical model predicts the effect of texture on RR quite

well. The adjustment factor captures the intercept's effect in addition to that of the surface texture's. Becasue the numerical model was not calibrated, there is a larger difference between the adjustment factors of the experimental and numerical models.

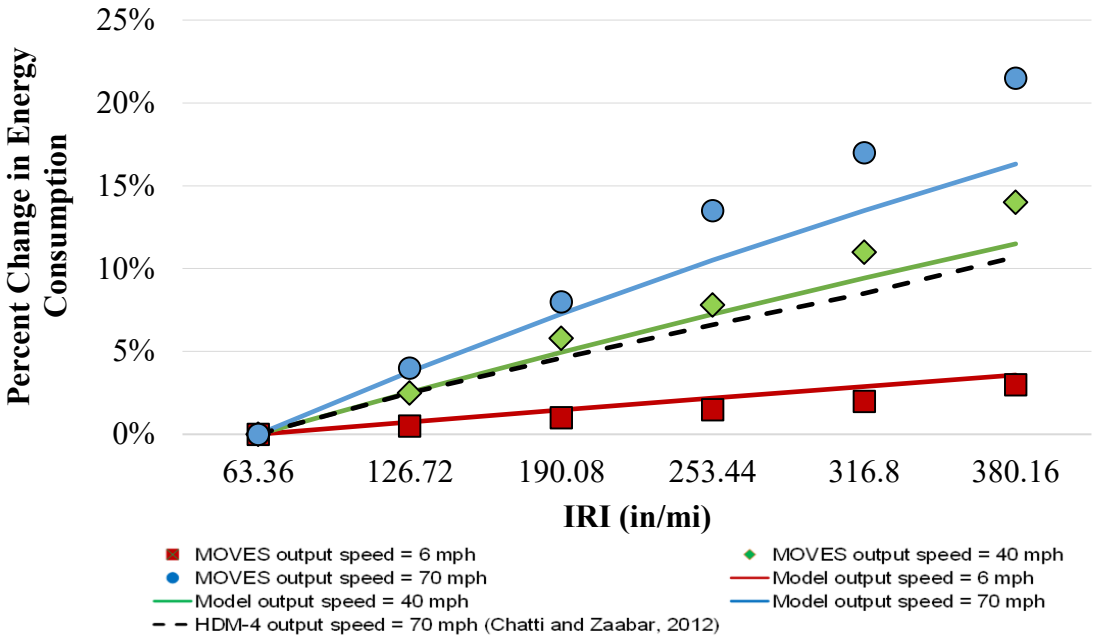

(a) Passenger Car

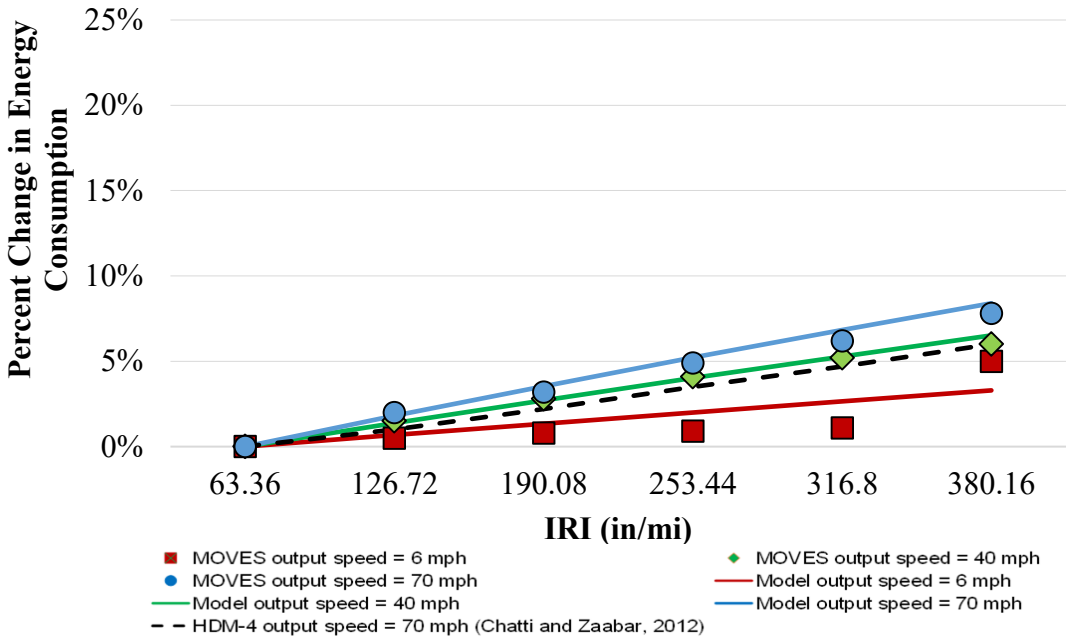

(b) Large Truck

Figure 2-1 Change in energy consumption for a (a) passenger vehicle and (b) large truck with increasing IRIs and speeds.

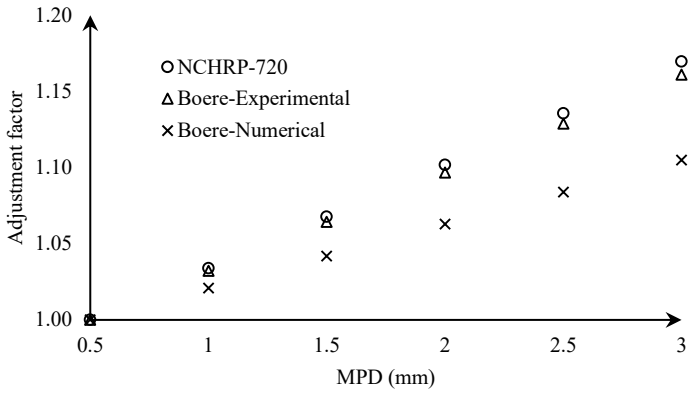

Figure 2-2 Comparison of RR models, including the NCHRP 720 report and the Boere experiment and numerical model for a light truck at v=50 mph.

Figure 2-3 presents the comparison of the adjustment factors for RR between the NCHRP 720 and MIRIAM models for a car (1.5t) as well as a heavy truck with a trailer (30t). The effect of texture is significantly higher in the MIRIAM model.

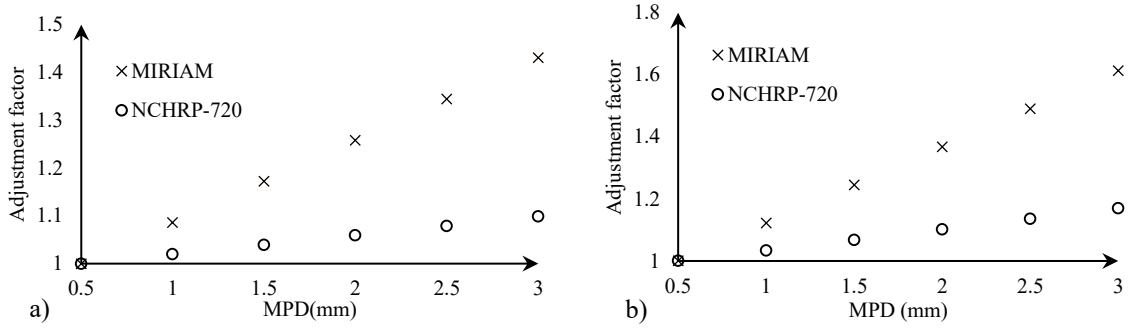

Figure 2-3 Comparison of RR models, specifically the NCHRP 720 report and the MIRIAM project for a (a) car and (b) a heavy truck with trailer.

The results from the NCHRP 720 model match the independent experimental results reported by Boere quite well, and they are in agreement with Boere's numerical model. On the other hand, the MIRIAM model gives a significantly higher texture effect than the NCHRP 720 model. Therefore, the NCHRP 720 and Boere models appear to be more reliable than the MIRIAM model, which overestimates the effect of texture on RR. Thus, this study used the NCHRP 720 model for the tool development.

CHAPTER 3 - USE STAGE PROGRESSION MODELS

3.1 INTERNATIONAL ROUGHNESS INDEX PROGRESSION

This study uses three progression models. All methods require different parameter inputs from the user.

3.1.1 Default Progression Model

The first model is known as the default progression model, which requires users to input both an initial and an upper threshold value for each treatment's IRI. Using a previously determined lifetime, a basic IRI progression can be extracted from the given information. An example is given in Table 3-1 (the start and end years are extracted from a previously determined lifetime) and Figure 3-1.

Table 3-1 Example IRI Progression Input Chart for Default Progression Model.

Treatment No.	Start Year	End Year	Initial IRI	Threshold IRI
1	0	5	80	150
2	5	12	90	150
3	12	19	75	150

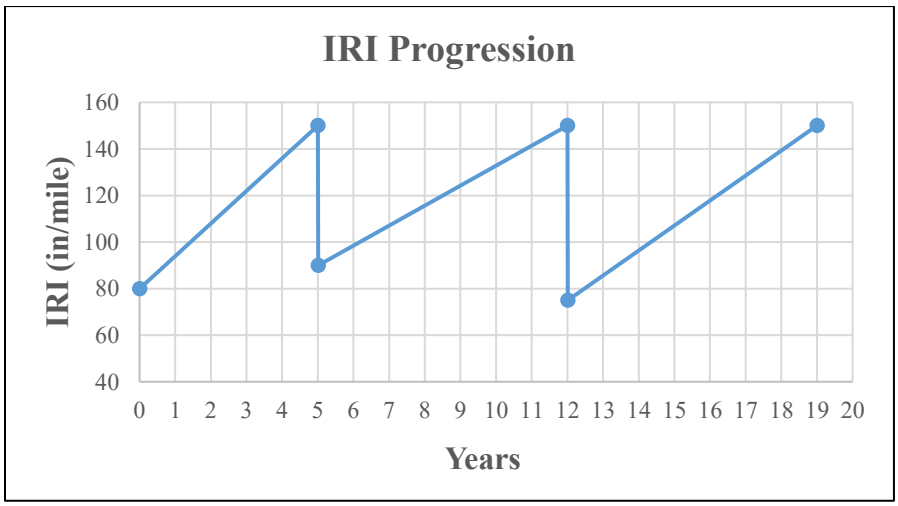

Figure 3-1 Example IRI progression plot for default progression model.

3.1.2 Basic Linear Progression Model

The basic linear model — the second model used in this study — also requires users to input the initial *IRI* for each treatment; however, instead of inputting an upper threshold value, it requires a global-progression rate in in/mi/yr.

The global progression rate ensures that the IRI progression maintains the same slope throughout each treatment cycle. An example is given in Table 3-2 and Figure 3-2.

Table 3-2 Example IRI Progression Input Chart for Basic Linear Progression Model

Treatment No.	Start Year	End Year	Initial IRI	Progression Rate
1	0	5	80	15
2	5	12	90	15
3	12	19	75	15

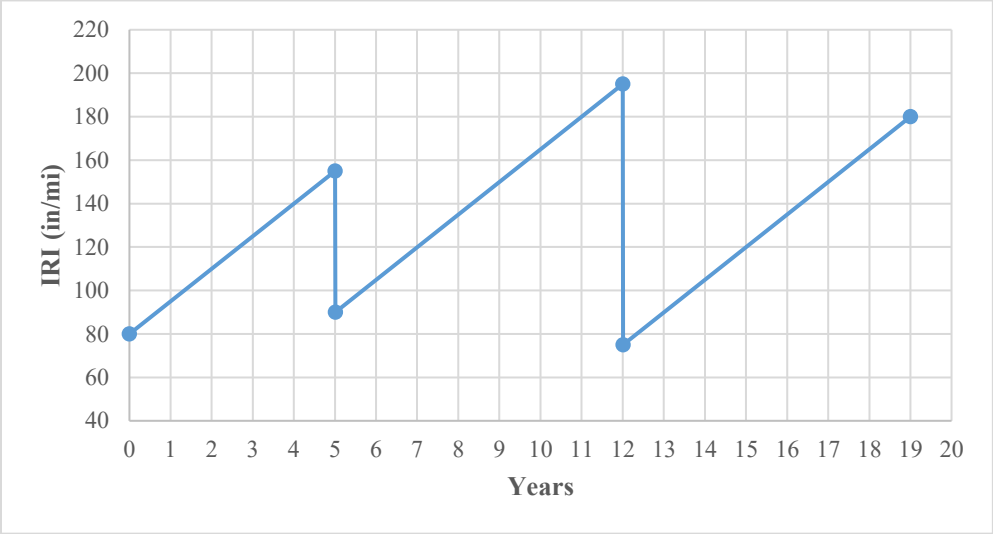

Figure 3-2 Example IRI progression plot for basic linear progression model.

3.1.3 Advanced Progression Model

The final progression model, the advanced progression model, uses the skeleton of the progression model, which was developed for Illinois Tollways (Al Qadi et al., 2015). The model captures the relationship between the IRI of two consecutive treatments and the drop in IRI right after a treatment. The model is as follows:

$$IRI_t = IRI_{t-1} + a * h^b * ESALs^c \tag{3.1}$$

$$IRI_{drop} = m * IRI_{before} + n \tag{3.2}$$

$$IRI_{after} = IRI_{before} - IRI_{drop} \tag{3.3}$$

where,

IRI_t = IRI value for year t, in/mi;
IRI_{t-1} = IRI value for year t-1, in/mi;.
h = thickness of a pavement's surface layer measured from field cores — in inches;
$ESALs$ = Equivalent single axle loads for the design lane in millions;
IRI_{before} = IRI value right before Maintenance;
IRI_{after} = IRI value right after Maintenance;
IRI_{drop} = $IRI_{before} - IRI_{after}$;
a, b, c = Coefficients for IRI progression model; and
m, n = Coefficients for IRI drop model

If the advanced progression model is selected, input all coefficients and parameters are required for the model. The coefficients used in the developed model are specific to Illinois Tollways (Al-Qadi et al., 2015). Volume I of the report includes example model coefficients for various case studies.

3.2 TEXTURE PROGRESSION

For texture progression, the MPD — measured in milometers — is a measure of pavement texture. A literature survey illustrated that MPD ranges from 0.2 to 3.8 mm (0.008 to 0.15 in) based on surface and treatment types. The summary of the literature survey is as follows:

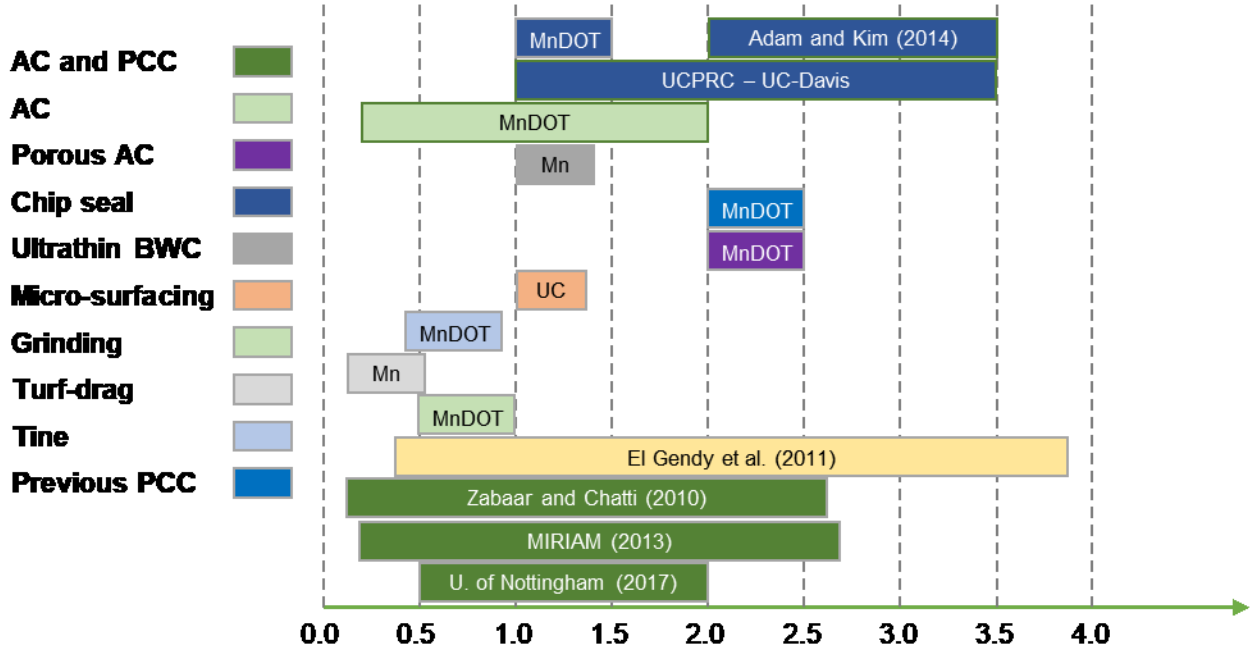

Figure 3-3 MPD ranges for various pavement surface types.

Based on the literature survey, this study compiled mean MPD values for various treatment types for both flexible and rigid pavements — all are presented in Table 3-3.

For flexible pavements, maximum MPD is observed with ½ -in chip seal, whereas fog seal had no effect on the mean MPD. As for rigid pavements, other than diamond grinding, treatment types have no effect on the mean MPD, which Table 3-3 illustrates.

For flexible pavements there are a few studies that investigate texture progression over time. Lu et al. (2009) investigated the MPD progression for various types of AC and rubberized AC. They observed that texture increased with time because of raveling.

Investigating the variation of surface texture with and without chip seal, Aavik et al. (2013) found that MPD decreased continuously without the presence of chip seal. With chip seal, the decrease in MPD stabilized after two years. However, there was not sufficient data to develop a progression model for chip seal (Aavik et al., 2013)

Table 3-3 Surface Texture for Various Treatments

Flexible Pavement		
Treatment Type		**Mean MPD**
Crack filling		Dependent on type and number of fills
Crack sealing		
Micro-surfacing		0.6
Thin AC overlay (less than 2.0 in)		0.52
CIR + thin AC overlay (less than 2.0 in)		0.52
CIR + medium AC overlay (2.0 to 4.0 in)		0.88
HIR + thin AC overlay (less than 2.0 in)		0.52
Slurry seal		0.5
Chip seal	1/4	1.2
	1/3	1.8
	3/8	1.98
	1/2	3.25
Ultra-thin bonded wearing course		1.15
Cape seal		Similar to slurry seal or micro-surfacing
Fog seal		No change
Bonded concrete overlays of asphalt		0.8
Rigid Pavement		
Surface Type		**Mean MPD**
Full-depth repair		No change
Full-depth repair with dowel-bar retrofitting		No change
Partial-depth repair		No change
Partial-depth repair with dowel-bar retrofitting		No change
Dowel-bar retrofitting		No change
Diamond grinding and grooving		0.95
Joint and crack resealing		No change

Li et al. (2013) investigated texture progression for each type of preservation treatment, but because data were collected for four months, it was impossible to develop a model. Therefore, no current studies may be used for developing a reliable texture progression model for flexible pavements.

For rigid pavements, Rao et al. (1999) investigated the effect of diamond grinding on surface texture. The researchers used the same road surface 10 years apart, and it was evident that rehabilitated lanes showed a different texture after 10 years. Since 10 years is a long time, no reliable model could be developed to quantify the change in texture with time.

In addition to the mentioned studies, the Long-Term Pavement Performance (LTTP) database was studied to investigate long-term texture progression. Ninety three sections in seven states have records of surface texture, and among these sections, 18 are AC or non-preservation overlays, seven are medium overlays, and seven are chip-seal sections, one is fog seal, 56 are PCC surfaces, two are grindings, and two are partial-depth patching of PCC.

The maximum measurement duration for MPDs is four years. Figure 3-4 shows samples of the MPD variation for these surfaces. As it can be seen, this database shows no specific trend for variation of surface texture. Main variations are related to surface type changes (Figure 3-4, b and c). Different factors, such as traffic and climate, have been considered for developing a model for these variations; however, this study found no reliable correlation based on this database.

From the aforementioned studies, it is evident that development of a model for surface texture variation with time may not be possible with the available database. However, for the long-term, LTTP data suggest a constant texture progression for many pavement surface types. Therefore, it is a valid assumption to only consider texture variation because of change in pavement surface type per the values provided in Table 3-3.

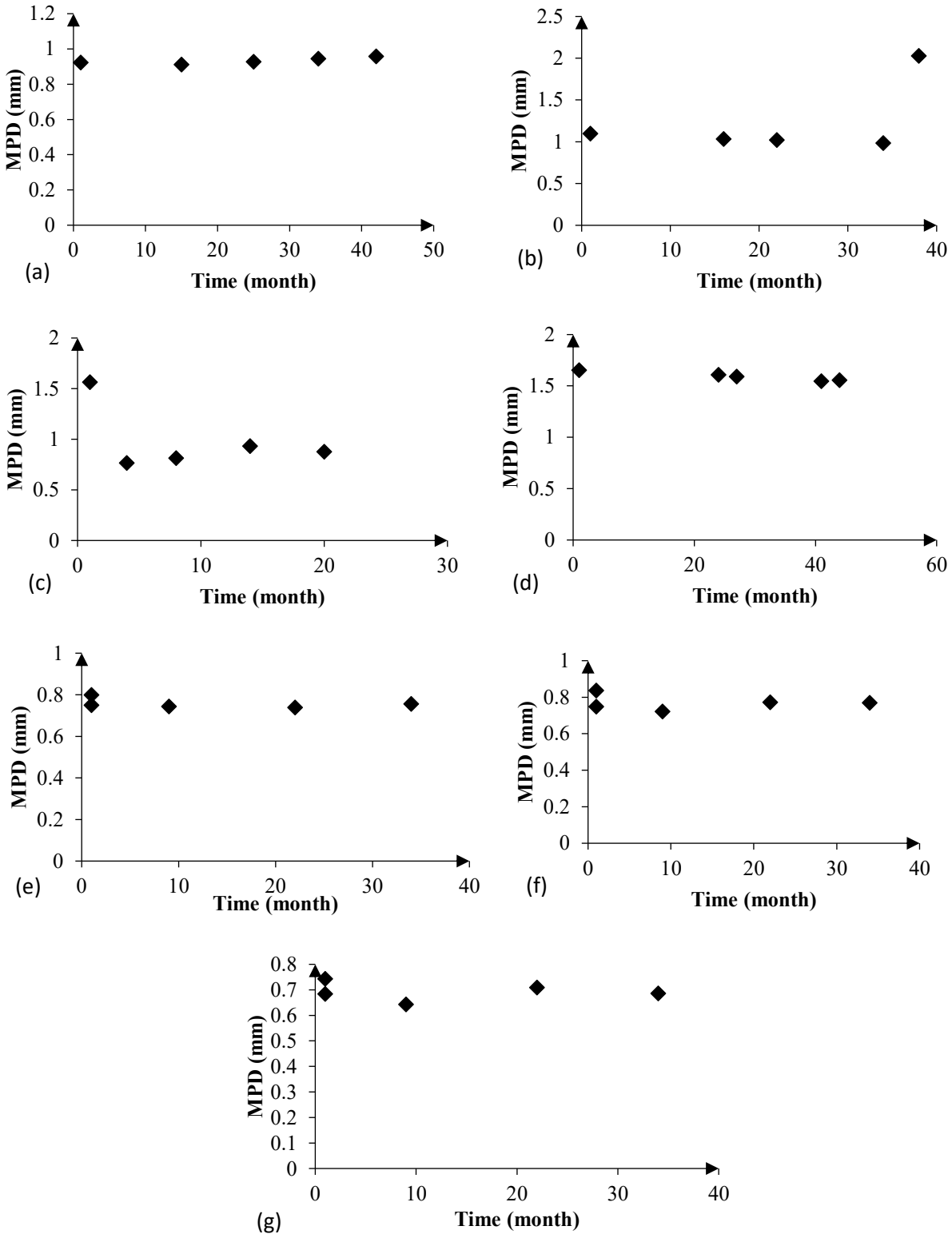

Figure 3-4 MPD variation for (a) medium overlay, (b) AC with chip seal, (c) AC with medium overlay, (d) fog seal, (e) concrete, (f) partial patching, and (g) diamond grinding from LTTP database

CHAPTER 4 - WORK ZONE MODELING

4.1 BACKGROUND

Many studies demonstrate that use stage dominates environmental impacts and energy consumption within pavement LCA (Huang and Parry, 2014). Traffic volume plays one of the most important roles in determining the use stage results. Therefore, delayed traffic induced by construction and maintenance activities may have significant effect on energy consumption and environmental impacts compared with those under normal traffic flow.

Work zones are defined as segments of highway where construction and maintenance operations reduce the number of lanes available to traffic, or they affect the operational characteristics of traffic flowing through the area (Wang, et al., 2014). The impact on traffic because of work zones is not completely inevitable when conducting LCA on a pavement project. Because work zones are time-limited, environmental impacts and energy consumption induced by them are not comparable with those in other life cycle stages.

This study, however, focuses on pavement preservation and maintenance activities, and it aims to design a more sustainable preservation and maintenance schedule. Each activity causes traffic delays; hence, it is important to consider work zone impacts when comparing different preservation and maintenance schedules.

4.2 WORK ZONE IMPACT

Work zone impacts may be assessed by calculating the different impacts induced by normal and delayed traffic flows, Figure 4-1. For example, in each work zone, the additional energy consumption calculation process can be represented by Equation 4.1. Similarly, the additional environmental impacts can also be calculated as Equation 4.2 shows.

$$\Delta E_{WZ} = E_{queue} + E_{WZ} + E_{Exit} - E_{Normal} \quad (4.1)$$

Where,

ΔE_{WZ} is additional energy consumption due to work zone;
E_{queue} is energy consumption resulting from traffic in queue zone;
E_{WZ} is energy consumption resulting from traffic in work zone;
E_{Exit} is energy consumption resulting from traffic in exiting zone; and
E_{Normal} is energy consumption resulting from traffic in a normal traffic.

$$\Delta Env^{i}_{WZ} = Env^{i}_{queue} + Env^{i}_{WZ} + Env^{i}_{Exit} - Env^{i}_{Normal} \quad (4.2)$$

Where,

ΔE^{i}_{WZ} is additional environmental impact due to work zone;
E^{i}_{queue} is environmental impact resulting from traffic in queue zone;
E^{i}_{WZ} is environmental impact resulting from traffic in work zone;
E^{i}_{Exit} is environmental impact resulting from traffic in exiting zone; and
E^{i}_{Normal} is environmental impact resulting from traffic in a normal traffic.

The RSI model (Equations 2.3 and 2.4) are used to determine the energy consumption and environmental impacts under different speeds and surface roughness levels. This method may be applied to calculate work zone impacts when the zone speed and length are known. In this study, the length and speed for queues and work zones as well as the work zone time are used as input.

The work zone calculation may be simplified by assuming no queue zone exists before the work zone and the work zone speed is 10 mph less than the normal speed. It is noted that the *IRI* value used in the RSI model is the average of *IRI* progression, defined in use-stage analysis, and the results are categorized by different vehicle types (i.e. passenger cars, small trucks, medium trucks, large trucks).

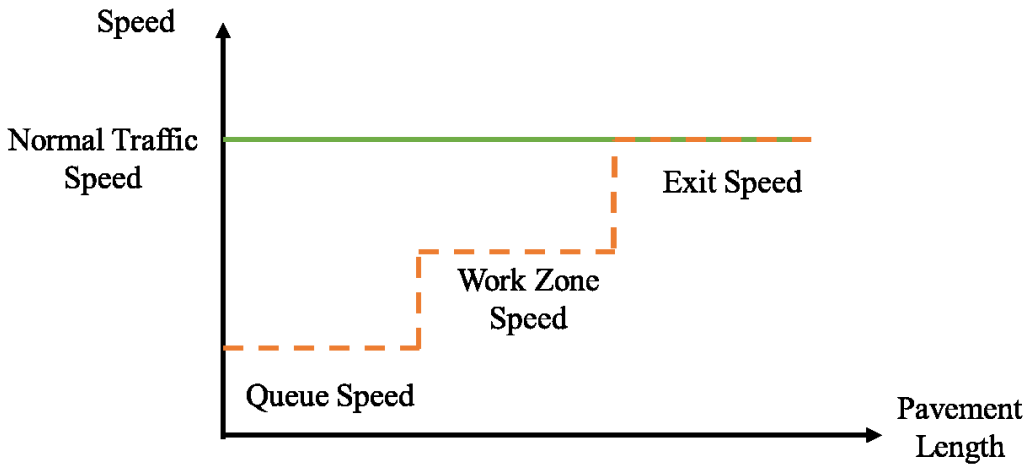

Figure 4-1 Work zone speed

CHAPTER 5 - CONCLUSIONS

The use stage models used in the preservation LCA tool are presented. The tool considers both the heat island impact and the rolling resistance effects.

To compute global warming potential, this study included in the analysis the radioactive pavement forcing for each state and the albedo values for each pavement surface type. Therefore, this research captured the heat island effect due to the change of surface after a preservation activity.

For rolling resistance, this report separated roughness and texture effects. As for the fuel consumption model resulted from roughness, this study used the RSI model to quantify the increase in fuel consumption due to the increase in roughness. For validation, the proposed model was compared to the HDM-4 and MOVES models. The IRI progression was captured by three various models: default, basic-linear, and advanced models. The user may select the model that fits project case.

Texture progression was assumed constant for the lifetime of the preservation activity; changes occur only after a preservation activity. The NCHRP-720 texture model was used to quantify the fuel consumption. The model was compared to those MIRIAM and Boere.

REFERENCES

Aavik, A., Kaal, T., and Jentson, M. (2013). Use of pavement surface texture characteristics measurement results in Estonia. *The XXVIII International Baltic Road Conference*. Vilnius, Lithuania.

Adams, J. M., and Richard Kim, Y. (2014). Mean profile depth analysis of field and laboratory traffic-loaded chip seal surface treatments. *International Journal of Pavement Engineering*. 15(7), 645-656.

Al-Qadi, I. L., Yang, R., Kang, S., Ozer, H., Ferrebee, E., Roesler, J. R., Salinas, A., Meijer, J., Vavrik, W. R., and Gillen, S. L. (2015). Scenarios developed for improved sustainability of Illinois Tollway: Life-cycle assessment approach. *Transportation Research Record*, 2523(1), 11-18.

Araújo, J. P., Oliveira, J. R., and Silva, H. M. (2014). The importance of the use phase on the LCA of environmentally friendly solutions for asphalt road pavements. *Transportation Research Part D: Transport and Environment*,32, 97-110. doi:10.1016/j.trd.2014.07.006

Boere, S. (2009). Prediction of road texture influence on rolling resistance. Eindhoven University of Technology.

Chatti, K. and Zaabar, I. (2012). Estimating the effects of pavement condition on vehicle operating costs. *NCHRP Report 720*. Transportation Research Board.

El Gendy, A., Shalaby, A., Saleh, M., and Flintsch, G. W. (2011). Stereo-vision applications to reconstruct the 3D texture of pavement surface. *International Journal of Pavement Engineering*, 12(03), 263-273.

Ghosh, L. E., Lu, L., Ozer, H., Ouyang, Y., & Al-Qadi, I. L. (2015). Effects of pavement surface roughness and congestion on expected freeway traffic energy consumption. *Transportation Research Record*, 2503(1), 10-19.

Gustafsson, S. E. (1991). Transient plane source techniques for thermal conductivity and thermal diffusivity measurements of solid materials. *Review of Scientific Instruments*, 62(3), 797-804.

Huang, Y., and Parry, T. (2014). Pavement life cycle assessment. In Climate Change, Energy, Sustainability and Pavements (pp. 1-40). Springer, Berlin, Heidelberg.

ISO. (2009). Passenger Car, Truck and Bus Tyres—Methods of Measuring Rolling Resistance—Single Point Test and Correlation of Measurement Results. ISO 28580.

Jackson, R.L., Willis, J.R., Arnold, M., and Palmer, C. (2011). "Synthesis of the Effects of Pavement Properties on Tire Rolling Resistance." NCAT Report 11-05.

Karlsson, R., Hammarström, U., Sörensen, H. and Eriksson, O. (2011). Road surface influence on rolling resistance. Coastdown measurements for a car and an HGV. *VTI Notat 24A*. The Swedish Road and Transport Research Institute. Linköping.

Lepert, P., & Brillet, F. (2009). The overall effects of road works on global warming gas emissions. Transportation Research Part D: Transport and Environment, 14(8), 576-584.

Li, H., Harvey, J. T., Thigpen, C., and Wu, R. (2013). Surface treatment macrotexture and bicycle ride quality (No. UCPRC-RR-2013-07).

Lu, Q., Kohler, E. R., Harvey, J. T., and Ongel, A. (2009). Investigation of noise and durability performance trends for asphaltic pavement surface types: three-year results.

Pérez-Martínez, P. J. (2012). Energy consumption and emissions from the road transport in Spain: A conceptual approach. *Transport, 27(4).* 383-396. doi:10.3846/16484142.2012.751051

Rao, S., Yu, H., Khazanovich, L., Darter, M., and Mack, J. (1999). Longevity of diamond-ground concrete pavements. *Transportation Research Record: Journal of the Transportation Research Board*, (1684), 128-136.

Sen, S., and Roesler, J. (2016). Aging albedo model for asphalt pavement surfaces. *Journal of Cleaner Production*, 117, 169-175.

Sen, S., and Roesler, J. (2017). Microscale heat island characterization of rigid pavements. *Transportation Research Record: Journal of the Transportation Research Board.* (2639), 73-83.

Wang, T., Kim, C., and Harvey, J. (2014). Energy consumption and Greenhouse Gas Emission from highway work zone traffic in pavement life cycle assessment. In International Symposium on Pavement Life Cycle Assessment, Davis, California, USA.

Ziyadi, M., Ozer, H., Kang, S., & Al-Qadi, I. L. (2018). Vehicle energy consumption and an environmental impact calculation model for the transportation infrastructure systems. *Journal of Cleaner Production*, 174, 424-436.